7

RF and Microwave Power Sensor Calibration by Direct Comparison Transfer

Yueyan Shan[1] and Xiaohai Cui[2]
[1]*National Metrology Centre, A*STAR*
[2]*National Institute of Metrology*
[1]*Singapore*
[2]*P.R. China*

1. Introduction

Many instruments can be used to measure radio frequency (RF) and microwave power. The most accurate one is a power sensor with a meter. The accuracy of RF and microwave power measurement depends on the accuracy of power sensor calibration. This chapter provides calibration methods of RF and microwave power sensor with system setup, modeling, equations, and analyses in different representations, traceability and measurement uncertainty evaluations. From the simple direct comparison transfer method, to the different improvements, and then the general analytical models, the methods provided in this chapter are useful for the guided-wave power sensor calibration in frequency range of a few MHz to several hundred GHz.

2. Microwave power standard and traceability of power sensor calibration

Although the chapter is focusing on the power sensor calibration, it has to talk about first the primary microwave power standard so that the traceability of power sensor calibration is clearly defined.

According to the definition, primary standard is derived directly in terms of base units of the International System of Units (SI). Now the prevalently accepted primary microwave power standard is the calorimeter or microcalorimeter, which is a substitution type of primary standard based on heat measurement (Brunetti & Vremera, 2003; Clague, 1995; Cui, X. & Crowley, T. P. (2011); Famton, 1990; JCGM 200:2008; Oldfield, 1989).

The primary microwave power standard determines the effective efficiency and calibration factor through DC power substitution to realize the traceability to SI units. Power is measured in terms of heat capacity and rate of temperature rise. When microwave power is applied to a terminating device or load through transmission line, the microwave energy is absorbed and converted to heat energy, causing the load temperature to change. Similarly, when DC power is applied to the same load, the DC energy is converted to heat, causing the load temperature to change. When the temperature change caused by the DC power is equivalent to that caused by the microwave power, the DC power can be used to precisely determine the corresponding microwave power. This is the principle of DC power substitution. The substitution technique obviates the need for detailed knowledge of heat losses and thermal capacities.

The terminating device may not react in the same way for microwave and DC power absorption, so the effective efficiency η_e is used to perform the correction. In equation (1), microwave power P_{HF} absorbed by the terminating device is calculated by dividing the substituted DC power P_{DC} by the effective efficiency η_e:

$$\eta_e = \frac{P_{DC}}{P_{HF}} \tag{1}$$

Since the effective efficiency is independent of the mismatch correction, the calibration factor K is used to describe both the effective efficiency η_e and mismatch Γ as follows:

$$K = \eta_e \times (1 - |\Gamma|^2) \tag{2}$$

The calibration factor K is generally used at the time of calibration transfer from a reference standard to an unknown microwave power sensor. It is the focus in the following sections.

The measurement uncertainty is a non-negative parameter characterizing the dispersion of the effective efficiency η_e or the calibration factor K being attributed to the standards. The uncertainty is evaluated using "law of propagation of uncertainty" following "Guide to the expression of Uncertainty in Measurement" (GUM) (JCGM 100:2008). Evaluation of measurement and calibration uncertainty by Monte Carlo Method (MCM) is to use Monte Carlo simulation in the uncertainty evaluation of output quantities based on "uncertainty probability distribution propagation" (JCGM 101:2008). The following sections will cover both methods for the measurement uncertainty evaluations.

The value of a primary standard is disseminated to a secondary standard through calibration or comparison. Then the reference standard and working power sensors will be calibrated for use. The measurement results through such relations as unbroken chain of calibrations establish the metrological traceability, each contributing to the measurement uncertainty. The traceability is illustrated in Fig. 1. Here for reference purpose we deliberately provide not only the hierarchy, but also the uncertainties typically related. The real uncertainties depend on the frequency band and each laboratory conditions.

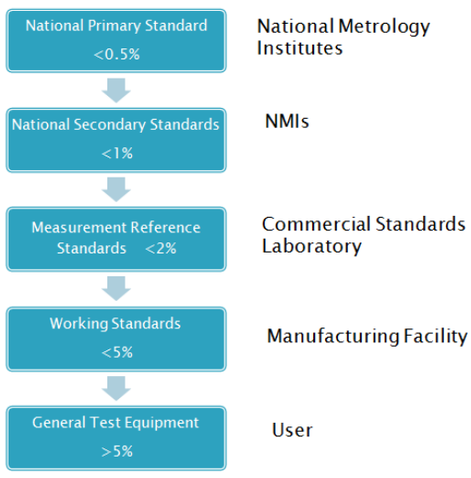

Fig. 1. Dissemination of primary standard to end user- Traceability Chart

3. Power sensor calibration by direct comparison transfer

3.1 Modeling

The calibration of RF and microwave power sensor is to transfer the effective efficiency or calibration factor from a primary standard to a secondary standard or from a secondary standard to a reference standard or from a reference standard to a power sensor. The parameter transfer is through comparison, or calibration one against the other. The simplest and the most obvious method to calibrate a power sensor against a reference standard is to connect each in turn to a stable power source, as illustrated in Fig. 2.

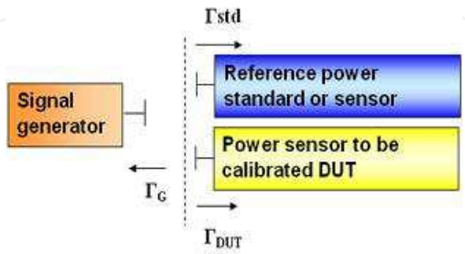

Fig. 2. Calibration of power sensor by the method of simple direct comparison transfer

Generally power from a source, $\boldsymbol{P}_i$, with reflection coefficient $\boldsymbol{\Gamma}_G$, incident to a load with reflection coefficient $\boldsymbol{\Gamma}_L$, can be expressed as follows (Agilent, 2003; Engen, 1993; Mial, 2007):

$$P_i = P_{Z_0} \times \frac{1}{|1 - \Gamma_G \Gamma_L|^2}$$

and a reflected power $\boldsymbol{P}_r$

$$P_r = P_{Z_0} \times \frac{\Gamma_L{}^2}{|1 - \Gamma_G \Gamma_L|^2}$$

For Fig. 2, the power dissipated to the reference power standard $\boldsymbol{P}_{Std}$, can be derived as

$$P_{Std} = P_i - P_{r,Std} = P_{Z_0} \times \frac{1 - |\Gamma_{Std}|^2}{|1 - \Gamma_G \Gamma_{Std}|^2}$$

And the power dissipated to the power sensor to be calibrated (DUT), $\boldsymbol{P}_{DUT}$, is as

$$P_{DUT} = P_i - P_{r,DUT} = P_{Z_0} \times \frac{1 - |\Gamma_{DUT}|^2}{|1 - \Gamma_G \Gamma_{DUT}|^2}$$

where P_{Z0} is the power available to a load with characteristic impedance Z_0. When idealized source with available power $\boldsymbol{P}_a$ has no internal impedance Z_0, $P_{Z0} = \boldsymbol{P}_a (1 - |\boldsymbol{\Gamma}_G|^2)$.

As shown in equation (1), the effective efficiency of a power sensor is a ratio. P_{DC} is DC or low frequency equivalent power, generating the same heat effect as the high frequency power being measured. For calibration of a power sensor, that is, to transfer the effective efficiency of a reference standard, η_{Std} , to a power sensor to be calibrated (DUT), η_{DUT}, it can be derived:

$$\frac{\eta_{DUT}}{\eta_{Std}} = \frac{\dfrac{P_{DC,DUT}}{P_{RF,DUT}}}{\dfrac{P_{DC,Std}}{P_{RF,Std}}} = \frac{\dfrac{P_{DC,DUT}}{P_{Z_0}\dfrac{1-|\Gamma_{DUT}|^2}{|1-\Gamma_G\Gamma_{DUT}|^2}}}{\dfrac{P_{DC,Std}}{P_{Z_0}\dfrac{1-|\Gamma_{std}|^2}{|1-\Gamma_G\Gamma_{std}|^2}}} = \frac{P_{DC,DUT}}{P_{DC,Std}} \times \frac{1-|\Gamma_{Std}|^2}{1-|\Gamma_{DUT}|^2}\frac{|1-\Gamma_G\Gamma_{DUT}|^2}{|1-\Gamma_G\Gamma_{Std}|^2}$$

So the calibration equation of effective efficiency for the method of Fig. 2 is expressed as:

$$\eta_{DUT} = \eta_{Std} \times \frac{P_{DC,DUT}}{P_{DC,Std}} \times \frac{1-|\Gamma_{Std}|^2}{1-|\Gamma_{DUT}|^2}\frac{|1-\Gamma_G\Gamma_{DUT}|^2}{|1-\Gamma_G\Gamma_{Std}|^2} \tag{3}$$

where η_{DUT} is the effective efficiency of DUT sensor.

This calibration equation involves three factors:

$$\eta_{DUT} = \eta_{Std} \times P_{RATIO} \times M_1 M_2$$

η_{Std} is the effective efficiency of a standard sensor. It comes from a national metrology institute, a calibration laboratory, or a manufacturer with traceability. P_{RATIO} is an equivalent DC or low frequency power ratio, depending on the system setup. M_1M_2 is the mismatch factor.

Similarly, calibration equation of calibration factor for the method of Fig. 2 is expressed as follows, considering equation (2):

$$K_{DUT} = K_{Std} \times \frac{P_{DC,DUT}}{P_{DC,Std}} \times \frac{|1-\Gamma_G\Gamma_{DUT}|^2}{|1-\Gamma_G\Gamma_{Std}|^2} \tag{4}$$

And the calibration factor transfer equation can also be expressed as three factors:

$$K_{DUT} = K_{Std} \times P_{RATIO} \times M$$

Notice that M is the mismatch factor for the calibration factor calibration transfer.

3.2 Uncertainty evaluation

From calibration transfer equation of effective efficiency (3) and that of calibration factor (4), if DUT power sensor has identical reflection coefficient as that of reference power standard, which means $\boldsymbol{\Gamma}_{DUT} = \boldsymbol{\Gamma}_{Std}$, each of them absorbs exactly the same amount of power from the source. Then by power ratio measurement it transfers the effective efficiency, $\boldsymbol{\eta_e}$, or calibration factor, K, from standard to DUT, to complete the calibration.

But the actual reflection coefficients of power sensors being compared usually differ significantly from one another (refer to Table 1). The signal generator reflection coefficient cannot dismiss easily. The complex items inside (3) and (4), i.e. the mismatch factors, cannot be neglected in accurate power sensor calibration with small uncertainty.

In recognition of the standards adopted internationally, the GUM (JCGM 100:2008) is considered as the basic technique to evaluate the uncertainty of measurement. The method proposed in the GUM is based on the law of propagation of uncertainty which is essentially the first-order Taylor series approximation of calibration equation, such as equation (4) of calibration factor. The partial differentiation of the output estimate with respect to the input estimates, which is termed sensitivity coefficient, is interpreted as a description of how the output estimate varies with changes in the values of the input estimates. The following equation is the definition of combined standard uncertainty $u_c(y)$ which includes both type A ($u_a(x)$) and type B ($u_b(x)$) uncertainties when the mathematical model is of the form $y = f(x_1, x_2, \ldots)$:

$$u_c(y) = \sqrt{u_a^2(x) + \sum_{i=1}^{N} \left(\frac{\partial f}{\partial x_i} \right)^2 u_b^2(x_i)} \tag{5}$$

Considering that the setup in Fig. 2 is the simple direct comparison transfer method, we present the uncertainty evaluation equations in different implementations, aiming at providing laboratories more realistic choices. The realistic magnitudes for reflection coefficients of instruments are used for the calculation and comparison. The specifications of reflection coefficients of the instruments quoted from different products at some frequency points are listed in Table 1.

	10 GHz			18 GHz			50 GHz			75GHz(wg)	
product	X	Y	Z	X	Y	Z	X	Y	Z	X	Y
sensor (Standard)	0.07	0.01	0.10	0.07	0.03	0.19	0.11	0.02	0.13	0.008	0.006
sensor (DUT)	0.11	0.13	0.16	0.11	0.09	0.06	0.11	0.13	0.20	0.029	0.038
signal generator	0.30	0.33	0.30	0.23	0.33	0.23	0.33	0.33	-	0.26	0.26

Table 1. Typical reflection coefficients of power sensors and signal generators

3.2.1 The simplest evaluation of measurement uncertainty

The simplest way in the calibration transfer of calibration factor from standard to DUT sensor is to simplify equation (4) to the following equation:

$$K_{DUT} = K_{Std} \times \frac{P_U}{P_S} = Ratio\ Factor \tag{6}$$

In which only the ratio factor is considered and set the mismatch factor M equal to 1. The real values of reflection coefficients are considered for the uncertainty budget only. In this case, the mismatch factor M for calibration factor K_{DUT} is expressed as:

$$M = \frac{M_U}{M_S}$$

where M_U and M_S are given by:

$$M_U = \left|1 - \Gamma_G \Gamma_{DUT}\right|^2 , \; M_S = \left|1 - \Gamma_G \Gamma_{Std}\right|^2$$

The associated uncertainties are calculated with the following equations (Agilent, 2003; Shan et al., 2010a):

$$u(M_X) = \sqrt{2}\,|\Gamma_G||\Gamma_X|; \quad X = Std,DUT \tag{7}$$

According to GUM for the law of propagation of uncertainties, the sensitivity coefficients are partial differentiations with respect to the individual variables in equation (6):

$$\frac{\partial K_{DUT}}{\partial K_{Std}} = \frac{P_U}{P_S} = \frac{K_{DUT}}{K_{Std}}$$

$$\frac{\partial K_{DUT}}{\partial P_U} = \frac{K_{Std}}{P_S} = \frac{K_{DUT}}{P_U} \tag{8}$$

$$\frac{\partial K_{DUT}}{\partial P_S} = -\frac{K_{Std} \times P_U}{P_S^2} = (-1)\frac{K_{DUT}}{P_S}$$

In which the expression is prepared for relative uncertainty representation since the combined standard uncertainty $u_c(y)$ can be expressed as an estimated relative combined variance $\left(\frac{u_c(y)}{y}\right)^2 = \sum_{i=1}^{N} P_i^2 \left(\frac{u(x_i)}{x_i}\right)^2$ when the mathematical model is of the form $Y = cX_1^{P_1} X_2^{P_2} \ldots X_N^{P_N}$.

The uncertainty budget is listed in Table 2 at frequency 18 GHz with type N connector. The calculations of mismatch uncertainties are based on Table 1 best and worst specifications.

It can be seen from Table 2 that the simplest evaluation of measurement uncertainty method is not an accurate method to obtain a small uncertainty. But it is useful for calibration laboratories with simple measurement set up as illustrated in Fig. 2. When this uncertainty value meets the demand, it is acceptable for industrial applications. In some evaluation experiments, it is also a practical method. Note that the value and uncertainty of a reference standard comes from the calibration of national metrology institutes or other calibration laboratories if the laboratory provides the calibration service using the method.

18 GHz	based on best specifications				
Quant.	Estim.	Standard uncertainty	probability distribution	Sensitivity coefficient	Uncertainty contribution
X_i	x_i	$u(x_i)$		c_i	$u_i(y)$
K_S	0.9894	0.0012	normal	1.0137	0.0012
M_S	1.0000	0.0098	U-shaped	1.0000	0.0098
M_U	1.0000	0.0195	U-shaped	1.0000	0.0195
P_U	1.0158	0.0018	normal	0.9873	0.0018
P_S	1.0021	0.0004	normal	-1.0008	-0.0004
$y=K_U$	1.0029				0.0219

18 GHz	based on worst specifications				
Quant.	Estim.	Standard uncertainty	probability distribution	Sensitivity coefficient	Uncertainty contribution
X_i	x_i	$u(x_i)$		c_i	$u_i(y)$
K_S	0.9894	0.0012	normal	1.0137	0.0012
M_S	1.0000	0.0887	U-shaped	1.0000	0.0887
M_U	1.0000	0.0513	U-shaped	1.0000	0.0513
P_U	1.0158	0.0018	normal	0.9873	0.0018
P_S	1.0021	0.0004	normal	-1.0008	-0.0004
$y=K_U$	1.0029				0.1025

Table 2. Uncertainty budget at 18 GHz for simplest evaluation of uncertainty for Fig. 2 measurement setup. Uncertainties u_i are at one standard deviation. Powers are measured in mW.

3.2.2 Measurement uncertainty improvement with mismatch correction

To improve the calibration accuracy and uncertainty evaluation, we have to perform a mismatch correction, i.e., the complex reflection coefficients have to be considered in the calibration model. The complex value is either representing in term of magnitude and phase or its real and imaginary components. In the majority of engineering applications, the magnitude and phase representation (Polar coordinates) is generally preferred because this representation bears a direct relationship to physical phenomena affecting the measurement process (Ridler & Salter, 2002). For example, phase relates directly to the electrical path length of a signal, and magnitude relates directly to the signal attenuation. The same cannot be said for the representation of real and imaginary components (Cartesian coordinates). If the scales are used to depict the different representations, the real and imaginary axes in the complex plane extend infinitely (±∞). It is the same as the scale is used to depict all real numbers which is routinely for the arithmetic operations. While the scales are used to represent magnitude and phase each possess a significant difference. The magnitude has a lower bound of zero below which values cannot exist, and phase is represented convertionally on a cyclical scale, either from -180^0 to $+180^0$ or from 0^0 to 360^0.

With mismatch correction added in computing the calibration factor using equation (4), the calculation of sensitivity coefficients involves the partial differentiations with respect to complex reflection coefficients. In the following sections, we separately provide the derived sensitivity coefficients in both Cartesian and Polar coordinate representations for practical measurement uncertainty solution and application; and also examples for their associated uncertainties are included. The derived sensitivity coefficients in both representations have been numerically appreciated by making use of MATLAB version R2010a, symbolic differentiation in Math Toolbox.

3.2.2.1 Cartesian representation of sensitivity coefficients for equation (4)

Representing calibration factor K_{DUT} of equation (4) with magnitude and phase components, it becomes

$$K_{DUT} = K_{Std} \times P_{RATIO} \times M = K_{Std} \times \frac{P_{DUT}}{P_{Std}} \times \frac{1+|\Gamma_{DUT}|^2|\Gamma_G|^2 - 2|\Gamma_{DUT}||\Gamma_G|\cos(\theta_{DUT}+\theta_G)}{1+|\Gamma_{Std}|^2|\Gamma_G|^2 - 2|\Gamma_{Std}||\Gamma_G|\cos(\theta_{Std}+\theta_G)} \quad (9)$$

Let M_N represent the numerator and M_D denominator of mismatch M:

$$M_N = |1 - \Gamma_{DUT}\Gamma_G|^2 = 1 + |\Gamma_{DUT}|^2|\Gamma_G|^2 - 2|\Gamma_{DUT}||\Gamma_G|\cos(\theta_{DUT} + \theta_G)$$

$$M_D = |1 - \Gamma_{Std}\Gamma_G|^2 = 1 + |\Gamma_{Std}|^2|\Gamma_G|^2 - 2|\Gamma_{Std}||\Gamma_G|\cos(\theta_{Std} + \theta_G)$$

Let $A=|\Gamma_G|$, $B=|\Gamma_{DUT}|$, $C=|\Gamma_{Std}|$, $D=\cos(\theta_{DUT}+\theta_G)$, $E=\cos(\theta_{Std}+\theta_G)$, and $Ratio\ Factor = K_{Std} \times \frac{P_{DUT}}{P_{Std}}$.

Then,

$$\begin{aligned} K_{DUT} &= K_{Std} \times P_{RATIO} \times M \\ &= Ratio\ Factor \times M = Ratio\ Factor \times \frac{1 + A^2B^2 - 2ABD}{1 + A^2C^2 - 2ACE} \end{aligned} \tag{10}$$

According to GUM for the law of propagation of uncertainties, the sensitivity coefficients are partial differentiations with respect to the individual variables in equation (10), total 9 items. The derived sensitivity coefficients are as follows:

1. The sensitivity coefficient for K_{Std}

$$\frac{\partial K_{DUT}}{\partial K_{Std}} = \frac{K_{DUT}}{K_{Std}} \tag{11}$$

2. The sensitivity coefficient for P_{DUT}

$$\frac{\partial K_{DUT}}{\partial P_{DUT}} = \frac{K_{DUT}}{P_{DUT}} \tag{12}$$

3. The sensitivity coefficient for P_{Std}

$$\frac{\partial K_{DUT}}{\partial P_{Std}} = -\frac{K_{DUT}}{P_{Std}} \tag{13}$$

4. The sensitivity coefficient for $|\Gamma_{Std}|$ (=C)

$$\frac{\partial K_{DUT}}{\partial |\Gamma_{Std}|} = -\frac{K_{DUT}}{M_D} \times 2A(AC - E) \tag{14}$$

5. The sensitivity coefficient for θ_{Std}

$$\frac{\partial K_{DUT}}{\partial \theta_{Std}} = -\frac{K_{DUT}}{M_D} \times 2AC\sin(\theta_{Std} + \theta_G) \tag{15}$$

6. The sensitivity coefficient for $|\Gamma_{DUT}|$ (=B)

$$\frac{\partial K_{DUT}}{\partial |\Gamma_{DUT}|} = Ratio\ Factor \times \frac{1}{M_D} \times 2A(AB - D) \tag{16}$$

7. The sensitivity coefficient for θ_{DUT}

$$\frac{\partial K_{DUT}}{\partial \theta_{DUT}} = Ratio\ Factor \times \frac{2AB}{M_D}\sin(\theta_{DUT} + \theta_G) \tag{17}$$

8. The sensitivity coefficient for $|\Gamma_G|$ (=A)

$$\frac{\partial K_{DUT}}{\partial |\Gamma_G|} = Ratio\ Factor \times \frac{2B}{M_D} \times (AB - D) - \frac{M_N \times 2C}{(M_D)^2} \times (AC - E) \tag{18}$$

9. The sensitivity coefficient for θ_G

$$\begin{aligned} \frac{\partial K_{DUT}}{\partial \theta_{DUT}} &= Ratio\ Factor \times \{\frac{2AB}{M_D}\sin(\theta_{DUT} + \theta_G) - \frac{M}{M_D} \times 2AC\sin(\theta_{Std} + \theta_G)\} \\ &= equation(17) + equation(15) \end{aligned} \tag{19}$$

3.2.2.2 Polar representation of sensitivity coefficients for equation (4)

Representing calibration factor K_{DUT} of equation (4) with real and imaginary components, the following denotation is used to denote the real and imaginary components of reflection coefficient:

$a = \mathrm{Re}\{\Gamma_{Std}\} = \Gamma_{Std\text{-}Re}$, $b = \mathrm{Im}\{\Gamma_{Std}\} = \Gamma_{Std\text{-}Img}$, $c = \mathrm{Re}\{\Gamma_{DUT}\} = \Gamma_{DUT\text{-}Re}$, $d = \mathrm{Im}\{\Gamma_{DUT}\} = \Gamma_{DUT\text{-}Img}$, $e = \mathrm{Re}\{\Gamma_G\} = \Gamma_{G\text{-}Re}$, and $f = \mathrm{Im}\{\Gamma_G\} = \Gamma_{G\text{-}Img}$

Then the calibration model becomes:

$$\begin{aligned} K_{DUT} &= K_{Std} \times P_{RATIO} \times M1 \\ &= Ratio\ Factor \times \frac{1 + 2df - 2ce + c^2e^2 + d^2e^2 + c^2f^2 + d^2f}{1 + 2bf - 2ae + a^2e^2 + b^2e^2 + a^2f^2 + b^2f^2} \end{aligned} \tag{20}$$

Let $M1_N$ represent the numerator and $M1_D$ denominator of mismatch $M1$ in real and imaginary format:

$$\begin{aligned} M1_N &= |1 - \Gamma_{DUT}\Gamma_G|^2 = 1 + 2df - 2ce + c^2e^2 + d^2e^2 + c^2f^2 + d^2f \\ M1_D &= |1 - \Gamma_{Std}\Gamma_G|^2 = 1 + 2bf - 2ae + a^2e^2 + b^2e^2 + a^2f^2 + b^2f^2 \end{aligned}$$

Similarly, according to GUM for the law of propagation of uncertainties, the sensitivity coefficients are partial differentiation with respect to each input quantities in equation (20), total 9 items. The derived sensitivity coefficients are as follows:

1. The sensitivity coefficients for K_{Std}, P_{DUT} , and P_{Std} are the same as those in equations (11), (12) and (13). But here K_{DUT} should use equation (20) instead.
2. The sensitivity coefficient for $\Gamma_{Std\text{-}Re}$ (= a) can be evaluated to obtain

$$\frac{\partial K_{DUT}}{\partial \Gamma_{Std\text{-}\mathrm{Re}}} = \frac{K_{DUT}}{M1_D} \times (2e - 2ae^2 - 2af^2) \tag{21}$$

3. The sensitivity coefficient for $\Gamma_{Std\text{-}Img}$ (= b)

$$\frac{\partial K_{DUT}}{\partial \Gamma_{Std\text{-}\mathrm{Im}g}} = \frac{K_{DUT}}{M1_D} \times \{(2f + 2be^2 + 2bf^2)\} \tag{22}$$

4. The sensitivity coefficient for $\Gamma_{DUT\text{-}Re}$ (= c)

$$\frac{\partial K_{DUT}}{\partial \Gamma_{DUT\text{-}\mathrm{Re}}} = Ratio\ Factor \times \frac{2e + 2ce^2 + 2cf^2}{M1_D} \tag{23}$$

5. The sensitivity coefficient for $\Gamma_{DUT\text{-}Img}$ (= d)

$$\frac{\partial K_{DUT}}{\partial \Gamma_{DUT\text{-}\mathrm{Im}g}} = Ratio\ Factor \times \frac{2f + 2de^2 + 2df^2}{M1_D} \tag{24}$$

6. The sensitivity coefficient for $\Gamma_{G\text{-}Re}$ (= e)

$$\frac{\partial K_{DUT}}{\partial \Gamma_{G\text{-}\mathrm{Re}}} = Ratio\ Factor \times \frac{2c + 2c^2e + 2d^2e + (M1)\left(2a - 2a^2e - 2b^2e\right)}{M1_D} \tag{25}$$

7. The sensitivity coefficient for $\Gamma_{G\text{-}Img}$ (= f)

$$\frac{\partial K_{DUT}}{\partial \Gamma_{G\text{-}\mathrm{Im}g}} = Ratio\ Factor \times \frac{2d + 2c^2f + 2d^2f - (M1)\left(2b + 2a^2f + 2b^2f\right)}{M1_D} \tag{26}$$

3.2.2.3 Example

With the same data as used in Table 2, the uncertainty budget is listed in Table 3 with mismatch corrections considered in the calibration equation.

18 GHz	based on best specifications				
Quant.	Estim.	Standard uncertainty	probability distribution	Sensitivity coefficient	Uncertainty contribution
X_i	x_i	$u(x_i)$		c_i	$u_i(y)$
K_{Std}	0.9894	0.0012	normal	0.9996	0.0012
P_{DUT}	1.0158	0.0018	normal	0.9737	0.0018
P_{Std}	1.0021	0.0004	normal	-0.9870	-0.0004
Γ_{DUTmag}	0.0600	0.0120	normal	-0.4613	-0.0055
$\Gamma_{DUTPhase}$	3.1416	1.5709	normal	0.0000	0.0000
Γ_{Stdmag}	0.0300	0.0060	normal	0.4581	0.0027
$\Gamma_{StdPhase}$	3.1416	1.5709	normal	0.0000	0.0000
Γ_{Gmag}	0.2300	0.0460	normal	-0.0606	-0.0028
Γ_{Gphase}	3.1416	1.5709	normal	0.0000	0.0000
$y=K_U$	0.9890				0.0071

18 GHz	based on worst specifications				
Quant.	Estim.	Standard uncertainty	probability distribution	Sensitivity coefficient	Uncertainty contribution
X_i	x_i	$u(x_i)$		c_i	$u_i(y)$
K_{Std}	0.9894	0.0012	normal	1.0716	0.0013
P_{DUT}	1.0158	0.0018	normal	1.0437	0.0019
P_{Std}	1.0021	0.0004	normal	-1.0580	-0.0004
Γ_{DUTmag}	0.1100	0.0220	normal	-0.7261	-0.0160
$\Gamma_{DUTPhase}$	3.1416	1.5709	normal	0.0000	0.0000
Γ_{Stdmag}	0.1900	0.0380	normal	0.7466	0.0284
$\Gamma_{StdPhase}$	3.1416	1.5709	normal	0.0000	0.0000
Γ_{Gmag}	0.3300	0.0660	normal	0.1878	0.0124
Γ_{Gphase}	3.1416	1.5709	normal	0.0000	0.0000
$y=K_U$	1.0602				0.0349

Table 3. Uncertainty budget at 18 GHz for measurement uncertainty improvement with mismatch correction for Fig. 2 measurement setup. Uncertainties u_i are at one standard deviation. Powers are measured in mW.

Compare the result in Table 3 with that in Table 2, the uncertainty is improved by mismatch correction. In the calculation, the magnitude uncertainty of reflection coefficient is assumed to be 40% of its value and the phase uncertainty is assumed to be 180^0 and value is π for all. In terms of computation cost, it is the same for both Cartesian and Polar coordinate representations. Note that additional uncertainties should also be included such as the connector repeatability, noise, cable flexibility, drift, linearity and frequency error when they are not negligible in practical application.

3.3 Discussions on simple direct comparison transfer

3.3.1 The pros and cons for simple direct comparison transfer

The above analyses based on the method illustrated in Fig. 2 are the simple direct comparison transfer calibration method. It is the most basic microwave power transfer technique. The system setup is fast, easy and simple.

But it is only for relatively rough measurement, since the reflection coefficient of a generator Γ_G, is more difficult to measure than that of a passive load. Γ_G varies with time and frequency. Many signal generators and amplifiers have non-linear output impedance. There are several developments on the measurement methods for Γ_G (Shimaoka et al., 2006; Torok et al., 2001) which is beyond the discussion of this chapter.

3.3.2 Improvement of direct comparison transfer by inserting passive components

To obviate the Γ_G, an intermediate component is proposed to use to increase the accuracy. If put an attenuator or an isolator on the source output, the reflection coefficient of a generator is improved. But low power is a problem for inserting an attenuator and being limited in frequency range is a problem for isolators (Rumfelt & Elwell, 1967).

A leveling circuit or ratio measurement can avoid the troubles. Resistive power splitter or directional coupler is normally used as the intermediate component and constructing the leveling circuit.

3.3.3 Splitter vs divider vs Tee: Scattering parameter matrix and suitable applications

Before going further analyses, it is time to say a few words about the power splitter (Johson, 1975), power divider and Tee since even some experienced engineers misuse them and not clear of the differences among them fundamentally. The physical and mathematical expressions are given here.

As illustrated in Fig. 3 for a) power divider; b) power splitter; and c) Tee, there are three resistors for power divider; two resistors for power splitter; and no resistors for Tee.

The three resisters in power divider are $Z_0/3$ each; for 50 ohm system, they are 16-2/3 Ω. Two resistors in power splitter are Z_0 each.

The power splitter has fixed input at port one; power divider and Tee inputs are exchangeable (bi-directional).

Substantially the scattering parameter matrix or S-parameter matrix are different for these three 3-port components as shown under the physical structures in Fig. 3; in which the S-parameter matrixes are for ideal cases.

Power splitter is used in leveling or ratio measurement; power divider is used for simple power division. Tee is used in low frequency case and in those non-critical measurements.

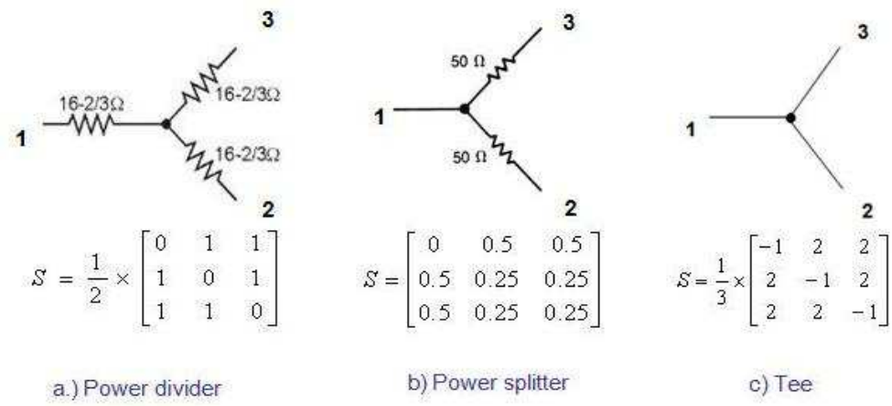

Fig. 3. Three 3-port components and their corresponding scattering parameter matrix

4. Coaxial splitter based power sensor calibration by direct comparison transfer

4.1 Benefit

The coaxial splitter based calibration setup is illustrated in Fig. 4. By using coaxial splitter in the direct comparison transfer method of RF and microwave power sensor calibration, the measurement accuracy improves from source mismatch effect and the load / device under test (DUT) mismatch effects. The explanations are as follows:

a. Improving source match is achieved by holding effective source output power constant. When a leveling loop or ratio sensor is employed, port 2 of the power splitter becomes the effective source output. Γ_{EG} is the equivalent source reflection coefficient rather than Γ_G, as illustrated in Fig. 5(a). It solves the measurement trouble of Γ_G for signal generator by obtaining passive component splitter S-parameters. The well known equivalent source reflection coefficient equation for power splitter

$$\Gamma_{EG} = S_{22} - S_{21}\frac{S_{32}}{S_{31}} \tag{27}$$

will be further discussed in section 6.

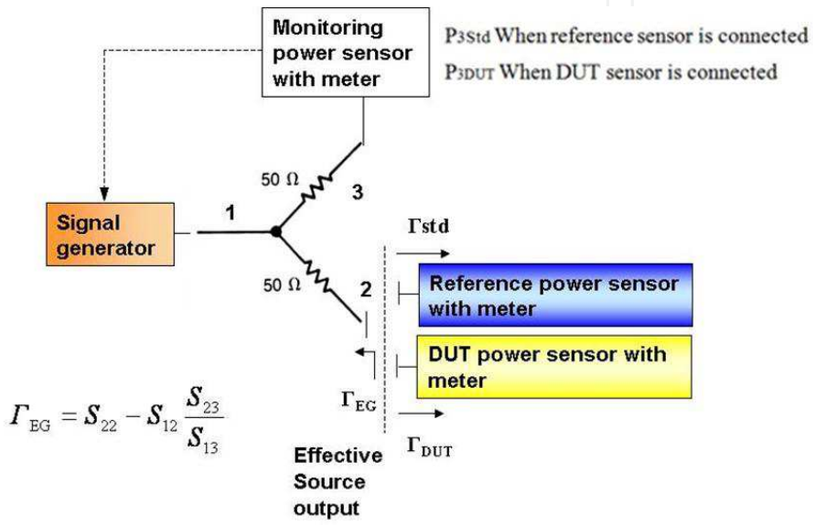

Fig. 4. Coaxial splitter based power measurement setup

b. As illustrated in Fig. 5(b), since S21 = S31, both arms 2 and 3 experience the same variation in input power, the leveling loop can compensate for any changes in effective source's output power.
c. As illustrated in Fig. 5(c) the leveling loop compensates for load variations as well. Since S22 = S32 it means that any changes in output power caused by the load reflection is also seen in the monitoring arm, permitting the leveling loop to compensate for these variations.

The source mismatch effect can be read through the monitoring arm, and so do the load / DUT mismatch effects. The system setup and mathematical model is established based on the complex reflection coefficients. Analyses have been provided through their S-parameter matrix to perform full mismatch corrections (Weidman, 1996; Juroshek, 2000; Ginley, 2006; Crowley, 2006; Shan et al., 2008; Shan et al., 2010b). Here we provide models for different cases in the application.

Since the splitter is not perfect, we seek to characterize them so that the mismatch error can be minimized by mathematical correction. The computation involved is not trivial, but the benefits of the technique are considerable, in that accurate measurements are made across a broad band without the need for mechanical adjustment.

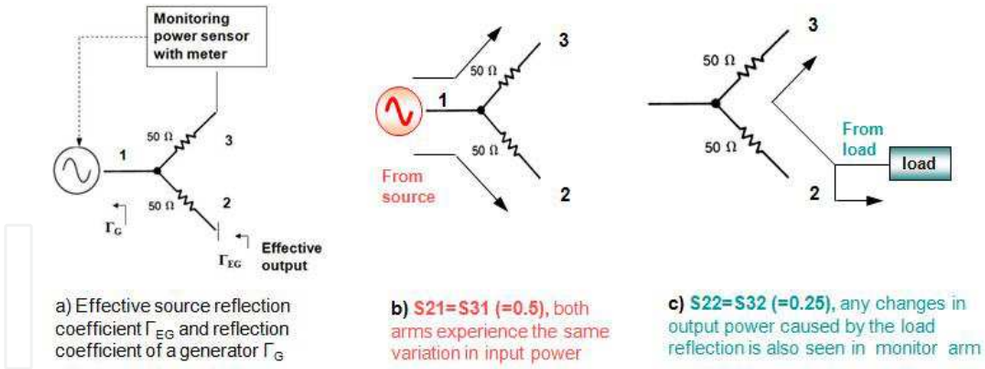

Fig. 5. Benefits by inserting coaxial power splitter

4.2 Modeling

Models of the three cases are considered for the system setup illustrated in Fig. 4.

Case 1 – obtain η_{DUT} from η_{Std}:

$$\eta_{DUT} = \eta_{Std} \times P_{RATIO} \times MM = \eta_{Std} \times \frac{P_{DUT}}{P_{Std}} \frac{P_{3Std}}{P_{3DUT}} \times \frac{1-|\Gamma_{Std}|^2}{1-|\Gamma_{DUT}|^2} \frac{|1-\Gamma_{DUT}\Gamma_{EG}|^2}{|1-\Gamma_{Std}\Gamma_{EG}|^2} \tag{28}$$

The Γ_{Std}, Γ_{DUT} and Γ_{EG} are the complex value reflection coefficients for the standard, DUT and equivalent signal generator respectively as indicated in Fig. 4. The power ratio is different from equation (3), which is caused by using splitter with monitoring arm. And here Γ_{EG} is used instead of Γ_G, different from simple direct comparison transfer. The value of Γ_{EG} is obtained by equation (27).

Case 2 – obtain K_{DUT} from K_{Std}:

$$K_{DUT} = K_{Std} \times \frac{P_{DUT}}{P_{Std}} \frac{P_{3Std}}{P_{3DUT}} \times \frac{|1-\Gamma_{DUT}\Gamma_{EG}|^2}{|1-\Gamma_{Std}\Gamma_{EG}|^2} \tag{29}$$

Case 3 – obtain K_{DUT} from η_{Std}:

$$K_{DUT} = \eta_{Std} \times \frac{P_{DUT}}{P_{Std}} \frac{P_{3Std}}{P_{3DUT}} \times (1-|\Gamma_{Std}|^2) \times \frac{|1-\Gamma_{DUT}\Gamma_{EG}|^2}{|1-\Gamma_{Std}\Gamma_{EG}|^2} \tag{30}$$

Case 3 is the practical application calibration equation in national metrology institutes. The obtained value from a primary standard is effective efficiency η_{Std}, the customer DUT calibration factor requests K_{DUT} .

In the following sections, we separately provide both Cartesian and Polar representations for practical solution and application.

4.3 Polar model

The models for the above three cases in terms of magnitude and phase is derived and expressed as follows:

$$\eta_{DUT} = \eta_{Std} \times \frac{P_{DUT}}{P_{Std}} \frac{P_{3Std}}{P_{3DUT}} \times \frac{1-|\Gamma_{Std}|^2}{1-|\Gamma_{DUT}|^2} \times \frac{1+|\Gamma_{DUT}|^2|\Gamma_{EG}|^2-2|\Gamma_{DUT}||\Gamma_{EG}|\cos(\theta_{DUT}+\theta_{EG})}{1+|\Gamma_{Std}|^2|\Gamma_{EG}|^2-2|\Gamma_{Std}||\Gamma_{EG}|\cos(\theta_{Std}+\theta_{EG})} \quad (31)$$

$$K_{DUT} = K_{Std} \times \frac{P_{DUT}}{P_{Std}} \frac{P_{3Std}}{P_{3DUT}} \times \frac{1+|\Gamma_{DUT}|^2|\Gamma_{EG}|^2-2|\Gamma_{DUT}||\Gamma_{EG}|\cos(\theta_{DUT}+\theta_{EG})}{1+|\Gamma_{Std}|^2|\Gamma_{EG}|^2-2|\Gamma_{Std}||\Gamma_{EG}|\cos(\theta_{Std}+\theta_{EG})} \quad (32)$$

$$K_{DUT} = \eta_{Std} \times \frac{P_{DUT}}{P_{Std}} \frac{P_{3Std}}{P_{3DUT}} \times (1-|\Gamma_{Std}|^2) \times \frac{1+|\Gamma_{DUT}|^2|\Gamma_{EG}|^2-2|\Gamma_{DUT}||\Gamma_{EG}|\cos(\theta_{DUT}+\theta_{EG})}{1+|\Gamma_{Std}|^2|\Gamma_{EG}|^2-2|\Gamma_{Std}||\Gamma_{EG}|\cos(\theta_{Std}+\theta_{EG})} \quad (33)$$

4.4 Uncertainty based on polar representation by Monte Carlo method

If using GUM to evaluate the uncertainty of measurement, it is based on propagation of uncertainties which is similar to analyses in previous section with more items. The mismatch uncertainty part is similar, just replace Γ_G with Γ_{EG}. It is seen from previous section that the sensitivity coefficients are quite tedious for complex value involved models although only first order summation of uncertainties are used. The derived sensitivity coefficients with partial differentiations with respect to each variable for the above models (31), (32) and (33) are obtained and have been numerically appreciated by making use of MATLAB. Here we discuss the Monte Carlo simulation Method (MCM). Then we compare the uncertainties by two methods and discuss the findings.

MCM is based on the propagation of distribution proposed by GUM supplement 1 (JCGM, 101:2008) instead of the GUM propagation of uncertainty method. The MCM allows one to get rid of much of the calculation of partial derivatives where analytical expressions are complex. The MCM evaluates measurement uncertainty by setting a probability function to each input quantity in the measurement equation. From a series of numerical calculations, probability density function (pdf) of the output function is obtained and the standard uncertainty is evaluated from this pdf.

The steps for applying MCM are summarized as follows:

Step 1. Select the number N of Monte Carlo Trials (iterations) to be made, with a given model Y, such as using equation (32). A value of 10^6 is often expected to deliver a 95% coverage interval for the output quantity.
Step 2. Generate N samples, by means of sampling from each input pdf. This N samples could be stored as a row vector in the program.
Step 3. For each of the input vector, form the output model Y, such as using equation (32).
Step 4. Sort the N evaluated values into a strict increasing order. Here, strict increasing requires all output values of Y to be unique. A good random generator in the program should satisfy this condition.
Step 5. With the sorted values, create a histogram for an approximation of the output pdf.
Step 6. Evaluate the estimate of the output model, given as y, and the standard uncertainty of y, given as u(y).
Step 7. Form a coverage interval for Y, given a required probability p. If the output pdf is symmetric, then the probabilistically symmetric interval is equal to the shortest coverage interval. Otherwise, shortest coverage interval has to be used.

The Monte Carlo numerical simulation is performed through program developed using MATLAB software. It allows estimating the measurement uncertainties based on the mathematical models.

4.5 Measurement system setup and type N connection result

The realization and implementation of coaxial splitter based power sensor calibration by direct comparison transfer shown in Fig. 4 is illustrated in Fig. 6 for the type N connector system setup (up to 18 GHz).

The calibration results of calibration factor of a power sensor with the measurement uncertainties are illustrated in Fig. 7. The DUT sensor is calibrated by a power standard (CN mount) in the frequency range 50 MHz to 18 GHz using the direct comparison transfer method with Weinshel 1870A splitter. The effective efficiency of power standard was measured using a micro-calorimeter. The calibration factor is calculated using equation (33). The expanded uncertainties are less than 0.9% for the frequency range at coverage factor of $k = 2$.

Compared with the results obtained in section 3, it is shown that with insertion of the passive splitter with monitoring arm, measurement uncertainties are much improved. And such measurement transfer system adds little measurement uncertainty when transfer the value from standard to DUT.

Uncertainty budget table is listed in Table 4 for the calibration system at frequency of 8 GHz.

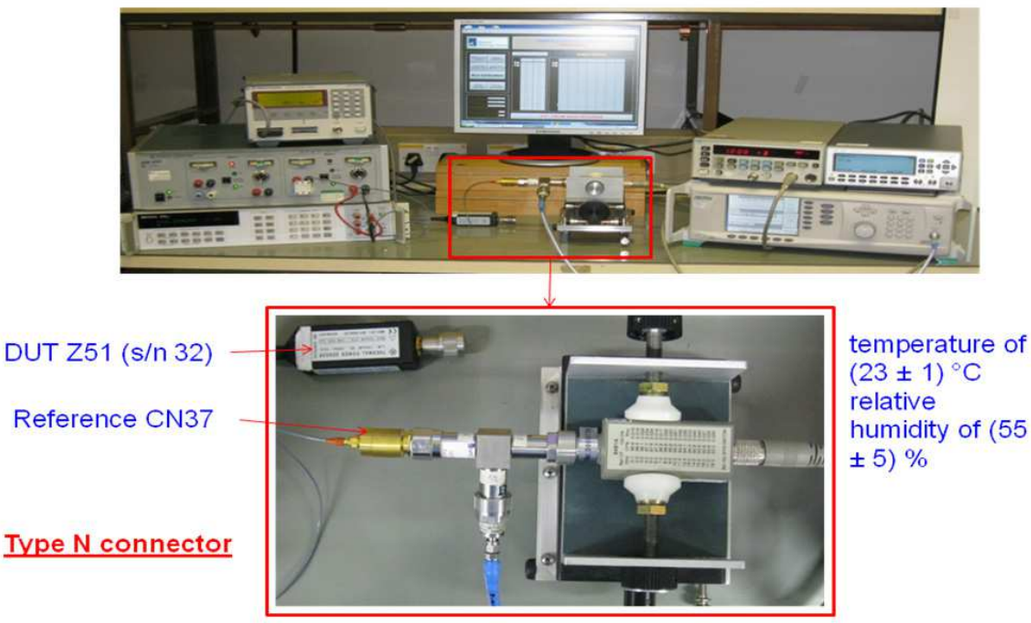

Fig. 6. Type N connection realization of splitter based power sensor calibration by direct comparison transfer

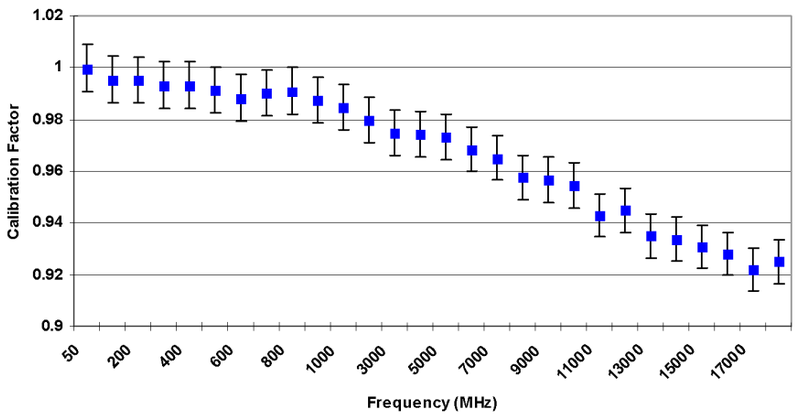

Fig. 7. measurement results by direct comparison method for power sensor 8481A vs CN

Quant.	Estim.	Standard uncertainty	probability distribution	Sensitivity coefficient	Uncertainty contribution
X_i	x_i	$u(x_i)$		c_i	$u_i(y)$
η_{Std}	0.9650	0.00165	normal	1.00617	0.00166
P_{Std}	0.9774	0.00036	normal	-0.99343	-0.00036
P_{DUT}	0.9886	0.00171	normal	0.98219	0.00168
P_{3Std}	1.0000	0.00010	normal	0.97099	0.00010
P_{3DUT}	1.0000	0.00010	normal	-0.97099	-0.00010
Γ_{Stdmag}	0.0466	0.00750	normal	-0.14611	-0.00110
$\Gamma_{StdPhase}$	-1.4228	0.18328	normal	-0.00269	-0.00049
Γ_{DUTmag}	0.0047	0.00750	normal	-0.07607	-0.00057
$\Gamma_{DUTPhase}$	2.8563	1.57088	normal	0.00012	0.00020
Γ_{EGmag}	0.0414	0.00751	normal	-0.07154	-0.00054
$\Gamma_{EGphase}$	-2.5226	0.18381	normal	-0.00257	-0.00047
$y=K_U$	**0.9678**				**0.0029**

Table 4. Uncertainty budget at 8 GHz for Fig. 4 measurement setup. Uncertainties u_i are at one standard deviation. Powers are measured in mW.

4.6 Cartesian model

Real and imaginary expression of the measurement models in the three cases are derived as follows:

$$\eta_{DUT} = \eta_{Std} \times \frac{P_{DUT}}{P_{Std}} \frac{P_{3Std}}{P_{3DUT}} \times \frac{1-A^2-B^2}{1-C^2-D^2} \times \frac{1+2DF-2CE+C^2E^2+D^2E^2+C^2F^2+D^2F}{1+2BF-2AE+A^2E^2+B^2E^2+A^2F^2+B^2F^2} \tag{34}$$

$$K_{DUT} = K_{Std} \times \frac{P_{DUT}}{P_{Std}} \frac{P_{3Std}}{P_{3DUT}} \times \frac{1+2DF-2CE+C^2E^2+D^2E^2+C^2F^2+D^2F}{1+2BF-2AE+A^2E^2+B^2E^2+A^2F^2+B^2F^2} \tag{35}$$

$$K_{DUT} = \eta_{Std} \times \frac{P_{DUT}}{P_{Std}} \frac{P_{3Std}}{P_{3DUT}} \times (1-A^2-B^2) \times \frac{1+2DF-2CE+C^2E^2+D^2E^2+C^2F^2+D^2F}{1+2BF-2AE+A^2E^2+B^2E^2+A^2F^2+B^2F^2} \tag{36}$$

where for all three cases, $\Gamma_{Std} = A + jB$, $\Gamma_{DUT} = C + jD$, $\Gamma_{EG} = E + jF$.

4.7 Measurement system for 2.4mm connection and comparison

The measurement setup for 2.4mm connector (up to 50 GHz) is illustrated in photo in Fig. 8. The calibration result is illustrated in Fig. 9. For uncertainty evaluation, the parameters used in the MCM are listed in Table 5. And the two columns in Table 6 compare the results obtained from GUM and MCM for selected frequency points.

Using Monte Carlo method, we generate a graphical approximation in the form of a histogram of the probability density function of the output quantity, represented in Fig. 10(a) with the frequency at 50 GHz. The uncertainty differences from the two methods for different frequency range are illustrated in Fig. 10(b). In this case, the uncertainties obtained by different methods are quite close. They can be used as the verification of the measurement uncertainty evaluations.

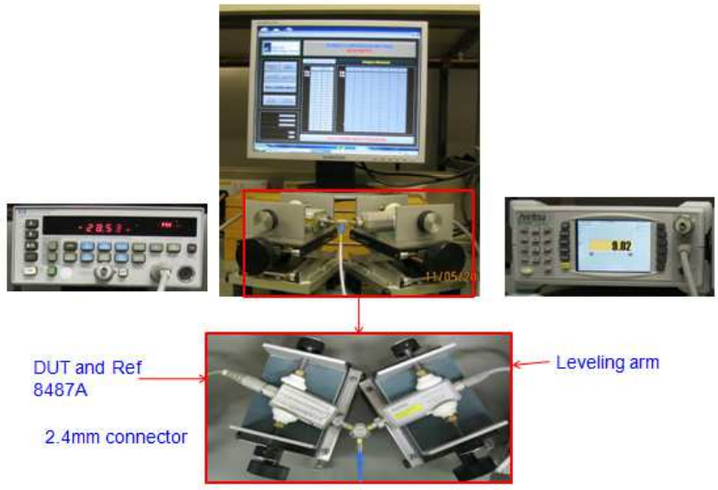

Fig. 8. 2.4mm connection realization of splitter based power sensor calibration by direct comparison transfer

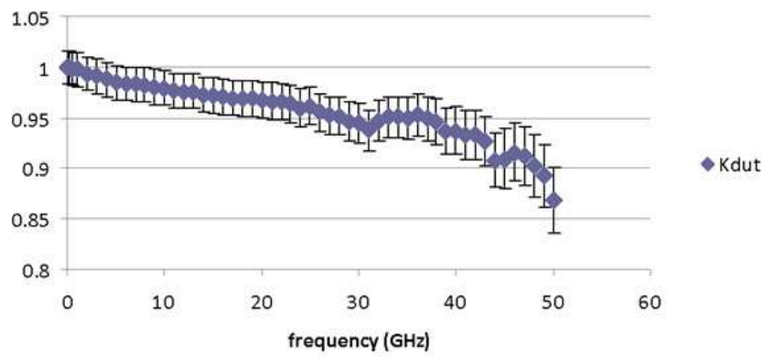

Fig. 9. 50 MHz to 50 GHz using the direct comparison transfer. The expanded uncertainties are less than 4% for the frequency range at k=2.

X_i	Distribution	Parameters	
		Expectation μ	Standard deviation σ
η_{Std}	$N(\mu,\sigma^2)$	0.9047	0.0158
P_{DUT}	$N(\mu,\sigma^2)$	8.4400e-04	1.0000e-06
P_{Std}	$N(\mu,\sigma^2)$	8.6200e-04	1.0000e-06
P_{3DUT}	$N(\mu,\sigma^2)$	9.9800e-04	1.0000e-07
P_{3Std}	$N(\mu,\sigma^2)$	1.0000e-03	1.0000e-07
$\lvert\Gamma_{DUT}\rvert$	$N(\mu,\sigma^2)$	0.1484	0.0125
θ_{DUT}	$N(\mu,\sigma^2)$	2.7501	0.1453
$\lvert\Gamma_{EG}\rvert$	$N(\mu,\sigma^2)$	0.1384	0.0125
θ_{EG}	$N(\mu,\sigma^2)$	2.6222	0.1448
$\lvert\Gamma_{Std}\rvert$	$N(\mu,\sigma^2)$	0.1288	0.0104
θ_{Std}	$N(\mu,\sigma^2)$	2.9504	0.0630

Table 5. Probability distribution parameters assigned to the individual input quantities at 50 GHz

Frequency = 50MHz		
	GUM	MCM
Mean	1.00854	1.008492
Stdev	0.008106	0.0076298
Lower Lim	0.992328	0.9935218
Upper Lim	1.024753	1.023428
Coverage Int	0.016212	0.0149531
Frequency = 50GHz		
Mean	0.874599	0.8728157
Stdev	0.01635	0.0154997
Lower Lim	0.841899	0.8423992
Upper Lim	0.907299	0.9031398
Coverage Int	0.032699	0.0303703

Table 6. Compares the results of different uncertainty evaluation methods for selected frequency points

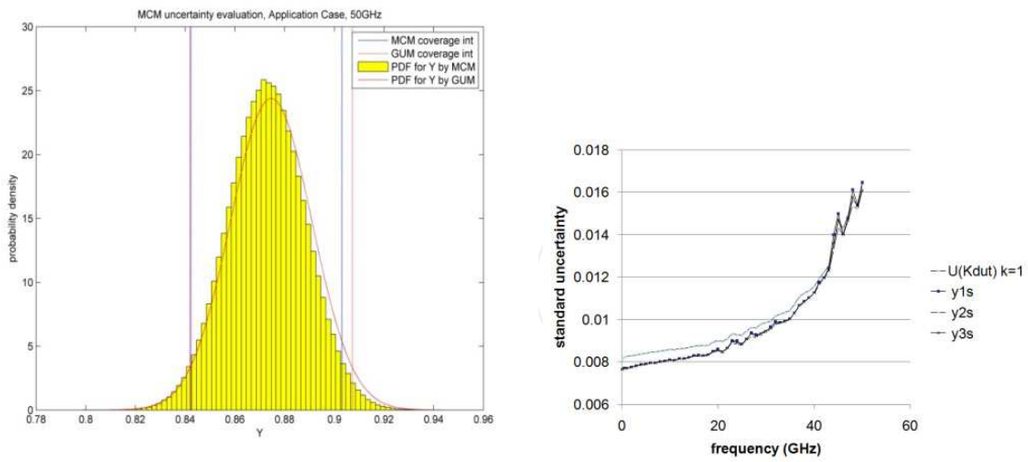

(a) (b)

Fig. 10. Comparison of uncertainty analyses by GUM and MCM

5. Generic models for power sensor calibration

5.1 Modeling with signal flow graph

For the sake of general purpose of application and analyses, in this section we discuss the three port structure expressed in signal flow graph. A flow graph method is particularly helpful in understanding a complex network relying on S-parameter matrix. Its correspondence with the physical behavior of the circuits allows simplification through well-founded approximations with no loss of physical insight (Bryant, 1993).

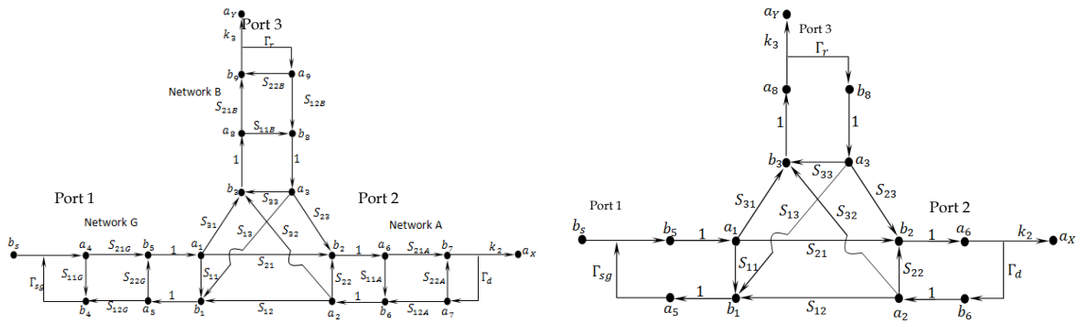

(a) (b)

Fig. 11. (a) Generic model signal flow graph for a 3-port structure. (b) Three two-port networks removed from Generic model

Referring to Fig. 11(a), the central part is signal flow graph for a general three port components, most commonly used are splitter and coupler. Three two-port networks, G, A and B, are added for the generic analysis. The signal source connected to port 1 is denoted by b_S.

5.2 Non-touching theory for the modeling analyses

The full power of flow graphs is evident only when they are combined with the non-touching loop rule. It is then possible to find the transfer function between any two nodes of a network almost by inspection. The complex wave functions a_i, b_i are the nodal points of signal flow along the paths designated by the arrows.

There are several special cases which are practically useful. We are going to discuss the following three cases.

5.3 Case study 1: Special case of the generic model comparing with section 4

When removing all the three two-port networks, G, A and B, the generic model is the special case as discussed in section 4. The generic model signal flow graph for a 3-port structure is then simplified as Fig. 11(b) (Wong, 2002).

The steps to evaluate the flow graph are summarized as follows:

There are two paths from b_s to a_x $P_1 = S_{21} \cdot k_2$ $P_2 = S_{31} \cdot \Gamma_r \cdot S_{23} \cdot k_2$
The transfer function is, $\frac{a_X}{b_s} = \frac{S_{21} \cdot k_2[1-(\Gamma_r \cdot S_{33})]}{1-\sum L(1)+\sum L(2)-\sum L(3)+\ldots} + \frac{S_{31} \cdot \Gamma_r \cdot S_{23} \cdot k_2[1-0]}{1-\sum L(1)+\sum L(2)-\sum L(3)+\ldots}$
There are two paths from b_s to a_Y $P_1 = S_{31} \cdot k_3$ $P_2 = S_{21} \cdot \Gamma_d \cdot S_{32} \cdot k_3$
The transfer function is, $\frac{a_Y}{b_s} = \frac{S_{31} \cdot k_3[1-\Gamma_d \cdot S_{22}]}{1-\sum L(1)+\sum L(2)-\sum L(3)+\ldots} + \frac{S_{21} \cdot \Gamma_d \cdot S_{32} \cdot k_3[1-0]}{1-\sum L(1)+\sum L(2)-\sum L(3)+\ldots}$
$\frac{a_X}{a_Y} = \frac{a_X}{b_s} \times \frac{b_s}{a_Y}$

Taking the ratio of a_X with respect to a_Y:

$$\frac{a_X}{a_Y} = \frac{a_X}{b_s} \times \frac{b_s}{a_Y} = \frac{k_2}{k_3}\left[\frac{S_{21}(1-\Gamma_r \cdot S_{33})+S_{31} \cdot \Gamma_r \cdot S_{23}}{S_{31}(1-\Gamma_d \cdot S_{22})+S_{21} \cdot \Gamma_d \cdot S_{32}}\right] = \left(\frac{k_2}{k_3}\right)\left(\frac{S_{21}}{S_{31}}\right)\left(\frac{1-\Gamma_r\left(S_{33}-\frac{S_{31}S_{23}}{S_{21}}\right)}{1-\Gamma_d\left(S_{22}-\frac{S_{21}S_{32}}{S_{31}}\right)}\right)$$

$$= \left(\frac{k_2}{k_3}\right)\left(\frac{S_{21}}{S_{31}}\right)\left(\frac{1-\Gamma_r\Gamma_{e3}}{1-\Gamma_d\Gamma_{e2}}\right) \tag{37}$$

Here k_2 and k_3 as illustrated in Fig. 11 are some unknown terms related to the cable and connector leakage, connection repeatability, drift, linearity and frequency error. And $\boldsymbol{\Gamma}_{e3}$ and $\boldsymbol{\Gamma}_{e2}$ are the so called equivalent source match terms of port 3 and port 2 respectively.

When the signal flow graph is used in power sensor calibration, recall that the power measured by a sensor P_m is actually $|b_i|^2$ times calibration factor K, i.e.

$$P_m = |b_i|^2 \times K \tag{38}$$

where $|b_i|^2$ is the power delivered to port *i* and *K* is the calibration factor.

Recall that in the measurement setup shown in Fig. 4, port 3 of the splitter is connected to a power sensor and meter, serving as a monitoring arm. Port 2 is a test arm, alternatively connected with standard and DUT power sensor. Power is measured at both port 2 and port 3.

When DUT is connected to the port 2, from equation (38) we can obtain the following ratio:

$$\frac{P_{DUT}}{P_{3DUT}} = \frac{|b_{2DUT}|^2 \times K_{DUT}}{|b_{3DUT}|^2 \times K_{3DUT}}$$

P_{DUT} and P_{3DUT} are the powers measured at port 2 when DUT power sensor connected and that at port 3 respectively. K_{DUT} and K_{3DUT} are the calibration factors corresponding to the respective DUT sensor and sensor connected at port 3. Then

$$K_{DUT} = K_{3DUT} \times \frac{P_{DUT}}{P_{3DUT}} \times \frac{|b_{3DUT}|^2}{|b_{2DUT}|^2} \tag{39}$$

Alternatively connection with port 2 is replaced with the standard power sensor. Port 3 remains as the monitoring arm. With the changes made at port 2, the similar ratio can be obtained, $\frac{P_{Std}}{P_{3Std}} = \frac{|b_{2Std}|^2 \times K_{Std}}{|b_{3Std}|^2 \times K_{3Std}}$ and

$$K_{Std} = K_{3Std} \times \frac{P_{Std}}{P_{3Std}} \times \frac{|b_{3Std}|^2}{|b_{2Std}|^2} \tag{40}$$

Since $K_{3Std} = K_{3DUT}$ for port 3 remains as the monitoring arm no matter port 2 connected with DUT or standard sensor, ratio of equation (39) and equation (40) yields

$$K_{DUT} = K_{Std} \times \frac{P_{DUT}}{P_{3DUT}} \times \frac{|b_{3DUT}|^2}{|b_{2DUT}|^2} \times \frac{P_{3Std}}{P_{Std}} \times \frac{|b_{2Std}|^2}{|b_{3Std}|^2} \tag{41}$$

Link to the transfer function derived in equation (37), and let $a_x = b_2$ and $a_y = b_3$

$$\frac{b_2}{b_3} = \frac{a_X}{a_Y} = \left(\frac{k_2}{k_3}\right)\left(\frac{S_{21}}{S_{31}}\right)\left(\frac{1-\Gamma_r\Gamma_{e3}}{1-\Gamma_d\Gamma_{e2}}\right) \tag{42}$$

Further modifications are made to equation (41) to specify the transfer function for the alternate connections of the standard power sensor and the DUT power sensor to port 2 of the splitter while port 3 remains as the monitoring arm. Then:

$$K_{DUT} = K_{Std} \times \frac{P_{DUT}}{P_{3DUT}} \times \frac{P_{3Std}}{P_{Std}} \times \left|\frac{k_{2Std}}{k_{2DUT}}\right|^2 \times \left|\frac{1-\Gamma_{DUT}\Gamma_{e2}}{1-\Gamma_{Std}\Gamma_{e2}}\right|^2 \tag{43}$$

Compare the derived equation (43) from signal flow graph Fig. 11(b) with equation (29) derived from Fig. 4, the only difference is $\left|\frac{k_{2Std}}{k_{2DUT}}\right|^2$ term. This term accounts for connector leakage, repeatability and so on. It is the Type A uncertainty shown in equation (5). The term is not explicitly expressed in the calibration equation (29). From different analytical method, we derive the same power sensor calibration equations.

5.4 Case study 2: Simultaneous comparison method analyses

Another way of using a resistive power splitter is the simultaneous comparison method. The reference standard and DUT power sensors to be calibrated are connected to the two output arms of the power splitter simultaneously. It seems an easy way of connection, no alternative connection of reference standard and DUT at port 2 of splitter as the above analyses. And there is application in some calibration laboratories.

With signal flow graph the transfer function can be easily obtained and reveal some findings. From equation (38), when DUT is connected to the port 2 and reference standard is connected to the port 3, we can obtain the following ratio:

$$\frac{P_{DUT}}{P_{3Std}} = \frac{|b_{2DUT}|^2 \times K_{DUT}}{|b_{3Std}|^2 \times K_{3Std}}$$

P_{DUT} and P_{3Std} are the powers measured at DUT power sensor connected to port 2 and the standard power sensor connected to port 3 respectively. K_{DUT} and K_{3Std} are the calibration factors corresponding to the respective sensors. Then

$$K_{DUT} = K_{3Std} \times \frac{P_{DUT}}{P_{3Std}} \times \frac{|b_{3Std}|^2}{|b_{2DUT}|^2} \tag{44}$$

Substitute equation (42) and simplify,

$$K_{DUT} = K_{Std} \times \frac{P_{DUT}}{P_{3DUT}} \times \left|\frac{k_{3Std}}{k_{2DUT}}\right|^2 \times \left|\frac{S_{31}}{S_{21}}\right|^2 \times \left|\frac{1-\Gamma_{DUT}\Gamma_{e2}}{1-\Gamma_{3Std}\Gamma_{e3}}\right|^2 \tag{45}$$

Compare equation (45) with equation (43), correction for mismatch when using the simultaneous comparison method is more complicated than for the direct comparison transfer method in which one port is used to monitor the signal level and the power sensors to be compared are connected in turn to the other output port. It can be seen from equation (45) that the mismatches at both output ports of the power splitter are needed to be taken into account. Unless perfect symmetry can be assumed, it is necessary to determine for each output port the value of Γ_{e3} and Γ_{e2} . For this reason the simultaneous comparison method is not often used for measurement where the highest precision is required. However the method is quite convenient if mismatch errors are not to be corrected for, provided that errors due to asymmetry are eliminated by interchanging the two power sensors to be compared.

5.5 Case study 3: Extend the model to waveguide application

As proved by equation (43), equation (29) actually can be extended to use for any three port structure, not only the coaxial splitter based calibration system. For waveguide power sensor calibration, the directional coupler replaces splitter as the media components. The same equation then is used for WR15 (50 GHz – 75 GHz) sensor calibration. The system setup is illustrated in Fig. 12.

6. Source mismatch determination and uncertainty

As mentioned in the beginning of section 4, the splitter provides small value of effective source reflection coefficient Γ_{EG} at its output port 2 when used in a leveling or ratio measurement mode. And Γ_{EG} can be calculated from its complex S-parameters by equation (27):

$$\Gamma_{EG} = S_{22} - S_{21}\frac{S_{32}}{S_{31}}$$

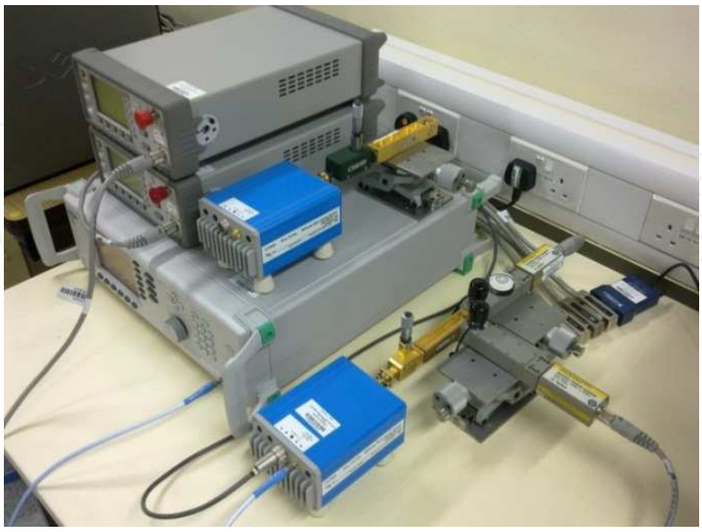

Fig. 12. Rectangular waveguide power sensor calibration system setup

One possible way of determining Γ_{EG} is to measure the splitter's complex S-parameters and calculate its value from equation (27). The measurement uncertainty in the S-parameters is then evaluated (EURAMET, 2011). Reference (Ridler and Salter, 2001) presented the law of propagation of uncertainty using matrix notation, treating the complex quantities with real and imaginary evaluation.

Since the calculation method from S-parameters is sensitive to small measurement errors, several different measurement methods were proposed, such as the "passive open circuit" and "active open circuit" method (Moyer, 1987), and the direct calibration method (Juroshek,1997). In the direct calibration method, the splitter is connected through ports 1 and 3 to a VNA. This effectively gives a new one port VNA at splitter port 2. This new VNA is calibrated using a one port calibration algorithm, e.g. short-open-load. The Γ_{EG} is then obtained as one of the three one-port VNA error terms. References (Rodriguez, 2000; Yhland & Stenarson, 2007) assessed the measurement uncertainty and traceability in power splitter effective source reflection coefficient. Reference (Furrer, 2007) compared direct calibration method with the calculation method. It seems that the similar results were obtained.

7. Conclusion

From simple direct comparison transfer method, to coaxial splitter based direct comparison transfer, and then to the general models with signal flow graph analyses, the chapter has meticulously discussed RF and microwave power sensor calibration methods. The models and equations provided target for practical usage. The examples and case studies have shown the practical applications. The traceability and measurement uncertainty with GUM and MCM have provided in details. The calibration models and methods described are useful for the coaxial and waveguide power sensor calibrations. The general models can be further developed for different case analyses in future studies.

8. Acknowledgement

The authors would like to thank the software and operation of their colleagues and students in the relative projects involved in the chapter.

9. References

Agilent, (2003). Application Note AN1449-1/2/3/4, *Fundamentals of RF and Microwave Power Measurements*, 2003-2011, Retrieved from: <www.agilent.com>

Brunetti, L. and Vremera, E. (2003). A new microcalorimeter for measurements in 3.5-mm coaxial line, *IEEE Transactions on Instrumentation and Measurement*, vol. 52, No. 2, pp. 320–323, Apr. 2003

Bryant, G. H. (1993). *Principles of Microwave Measurements*, revised Edition, pp.20-38, published by Peter Peregrinus Ltd., ISBN 0 86341 296 3, London, UK

Clague, F. R. (1995). *A Calibration Service for Coaxial Reference Standards for Microwave Power, NIST Technical Note 1374*, May 1995

Crowley, T. (2006). Microwave Power Measurement, NIST/ARFTG Measurement short course, 2006

Cui, X. and Crowley, T. P. (2011). Comparison of experimental techniques for evaluating the correction factor of a rectangular waveguide microcalorimeter", IEEE Transactions on Instrumentation and Measurement, Vol.60, No.7, pp.2690-2695, July 2011

Engen, G. F. (1992). *Microwave circuit theory and foundations of microwave metrology*, published by Peter Peregrinus Ltd, ISBN 0 86341 287 4, London, UK

EURAMET/cg-12/v.02, (2011). *Guidelines on the Evaluation of Vector Network Analyzers (VNA)*, Retrieved from: <http://www.euramet.org/index.php?id=calibration-guides>

Famton, A. (1990). *Radio Frequency & Microwave Power Measurement*, published by Peter Peregrinus Ltd, ISBN 0 86341 120 7, London, UK

Furrer, J. (2007). Comparison of 50 GHz Splitter Source Match Measurement Methods (Juroshek / Russell-hp), RF-Power Lab, METAS, 1.11.2007

Ginley, R. (2006). A direct comparison system for measuring radio frequency power (100 kHz to 18 GHz), *MEASURE*, pp.46-49, Vol.1, No.4, December 2006

Joint Committee for Guides in Metrology (JCGM) 100:2008. *Evaluation of measurement data – Guide to the expression of uncertainty in measurement*. Copyright of the document is shared jointly by the JCGM member organizations (BIPM, IEC, IFCC, ILAC, ISO, IUPAC, IUPAP and OIML). Retrieved from: <http://www.iso.org/sites/JCGM/GUM-introduction.htm>

JCGM 101:2008. *Evaluation of measurement data – Supplement 1 to the 'Guide to the Expression of Uncertainty in Measurement – Propagation of Distributions using a Monte Carlo method'*. Copyright of the document is shared jointly by the JCGM member organizations (BIPM, IEC, IFCC, ILAC, ISO, IUPAC, IUPAP and OIML). Retrieved from: <http://www.iso.org/sites/JCGM/GUM-introduction.htm >

JCGM 200:2008. *International Vocabulary Of Metrology – Basic and General Concepts and Associated Terms (VIM)*, Copyright of the document is shared jointly by the JCGM member organizations (BIPM, IEC, IFCC, ILAC, ISO, IUPAC, IUPAP and OIML). Retrieved from <http://www.iso.org/sites/JCGM/VIM-introduction.htm>

Johnson, R. A. (1975). Understanding Microwave Power Splitters, *Microwave Journal*, pp.49-56, December 1975

Juroshek, J. R. (1997). A direct calibration method for measuring equivalent source mismatch, *Microwave Journal*, pp. 106-118, Oct. 1997

Juroshek, J. R. (2000). NIST 0.05-50 GHz direct comparison power calibration system, *Conference on Precision Electromagnetic Measurements (CPEM2000)*, pp.166-167, 14-19 May 2000, Sydney, Australia

Mial, J. (2007). Chapter 15 : RF power measurement, In: *Microwave Measurements*, 3rd edition, Edited by R.J. Collier and A.D. Skinner, pp.330-348, published by The Institution of Engineering and Technology, ISBN 978-0-86341-735-1, London, UK

Moyer, R. D. (1987). Techniques for Measuring the effective source reflection coefficient of two-resistor power splitters, *IEEE Transactions on Instrumentation and Measurement,* pp.23-28, Vol.IM-36, No.1, March 1987

Oldfield, L.C. (1989). Chapter 7, Power measurement, In: *Microwave Measurement*, Edited by Bailey, A.E., second edition, pp. 105-131, published by Peter Peregrinus Ltd, ISBN 0 86341 184 3, London, UK

Ridler, N. M. and Salter, M. J. (2001). Propagating *S*-parameter uncertainties to other measurement quantities, *58th Automatic RF Techniques Group (ARFTG) conference*, November 2001

Ridler, N. M. and Salter, M. J. (2002). An approach to the treatment of uncertainty in complex *S*-parameter measurements, *Metrologia,* pp.295-302, Vol.39, No.3, 2002

Rodriguez, M. (2000). Towards Traceability of the direct calibration method to the cal kit standards, *Conference on Precision Electromagnetic Measurements (CPEM2000)*, pp.636-637, 14-19 May 2000, Sydney, Australia

Rumfelt, A. Y. and Elwell, L.B. (1967). Radio Frequency Power Measurements, *Proceedings of the IEEE*, pp.837-850, Vol.55, No.6, June 1967

Shan, Y., Chua, S.W., Neo H. and Wu, T. (2008). A Direct Comparison Transfer Microwave Power Sensor Calibration System, *Conference on Precision Electromagnetic Measurements (CPEM08)*, pp 512-513, 8-13 June 2008, Colorado USA

Shan, Y., Chua, S.W., Brunetti, L., Oberto, L. and Sellone, M. (2010a). Bilateral Comparison Between NMC And INRIM On Microwave Power Sensor Using Type N And 3.5 mm Connectors, *Conference On Precision Electromagnetic Measurements (CPEM2010)*, pp.736-737, 13-18 June, 2010, Daejeon, Korea

Shan, Y., Chua, S.W. and Yan, Y.K. (2010b). Development of A 50 GHz Coaxial Direct Comparison Transfer Microwave Power Sensor Calibration System At NMC, *Conference On Precision Electromagnetic Measurements (CPEM2010)*, pp.738-739, 13-18 June, 2010, Daejeon, Korea

Shimaoka, K., Shida, M. and Komiyama, K. (2006). Source reflection coefficient measurements of the power reference of power meters, CPEM2006, pp.664-665

Torok, A., Janik, D., Peinelt, W., Stumpe, D., and Stumper, U. (2001). Efficient Broadband method for equivalent source reflection coefficient measurements, *IEEE Transactions on instrumentation and measurement,* pp.361-363, Vol.50, No. 2, April 2001

Weidman, M.P. (1996). *Direct Comparison Transfer of Microwave Power Sensor Calibration, NIST Technical Note 1379*, January 1996

Wong, K. (2002). Power Sensor Calibration and Uncertainties, *60th ARFTG Conference*, December 2002

Yhland, K. and Stenarson, J. (2007). Measurement Uncertainty in Power Splitter Effective Source Match, *IEEE Transactions on Instrumentation and Measurement*, pp.669-672, Vol.56, No.2, April 2007

Modern Metrology Concerns

Edited by Dr. Luigi Cocco

ISBN 978-953-51-0584-8
Hard cover, 458 pages
Publisher InTech
Published online 16, May, 2012
Published in print edition May, 2012

"What are the recent developments in the field of Metrology?" International leading experts answer this question providing both state of the art presentation and a road map to the future of measurement science. The book is organized in six sections according to the areas of expertise, namely: Introduction; Length, Distance and Surface; Voltage, Current and Frequency; Optics; Time and Relativity; Biology and Medicine. Theoretical basis and applications are explained in accurate and comprehensive manner, providing a valuable reference to researchers and professionals.

How to reference

In order to correctly reference this scholarly work, feel free to copy and paste the following:

Yueyan Shan and Xiaohai Cui (2012). RF and Microwave Power Sensor Calibration by Direct Comparison Transfer, Modern Metrology Concerns, Dr. Luigi Cocco (Ed.), ISBN: 978-953-51-0584-8, InTech, Available from: http://www.intechopen.com/books/modern-metrology-concerns/rf-and-microwave-power-sensor-calibration-by-direct-comparison-transfer

INTECH
open science | open minds

InTech Europe
University Campus STeP Ri
Slavka Krautzeka 83/A
51000 Rijeka, Croatia
Phone: +385 (51) 770 447
Fax: +385 (51) 686 166
www.intechopen.com

InTech China
Unit 405, Office Block, Hotel Equatorial Shanghai
No.65, Yan An Road (West), Shanghai, 200040, China
中国上海市延安西路65号上海国际贵都大饭店办公楼405单元
Phone: +86-21-62489820
Fax: +86-21-62489821

IntechOpen